Ceramics International 48 (2022) 6750–6757

Contents lists available at ScienceDirect

Ceramics International

journal homepage: www.elsevier.com/locate/ceramint

Controlling anisotropy of porous B_4C structures through magnetic field-assisted freeze-casting

Said Bakkar [a,1,*], Saket Thapliyal [a], Nicholas Ku [b], Diana Berman [a], Samir M. Aouadi [a], Raymond E. Brennan [b], Marcus L. Young [a,**]

[a] Department of Material Science and Engineering, University of North Texas, Denton, TX, USA
[b] U.S. Army Research Laboratory, Aberdeen Proving Ground, MD, USA

ARTICLE INFO

Keywords:
Magnetic freeze-casting
B_4C
Porous ceramics

ABSTRACT

Anisotropic porous boron carbide (B_4C) structures were successfully produced, for the first time, using the magnetic field-assisted freeze casting method. The effect of the magnetic field on the structure and mechanical strength of the formed porous B_4C was compared for two different magnetic field directions that were either aligned with ice growth (vertical), or perpendicular to the ice growth direction (horizontal). It was shown that applying even a weak horizontal magnetic field of 0.1–0.3 T noticeably affected the alignment of mineral bridges between lamellar walls. Both the porosity and the channel widths decreased with increasing horizontal magnetic field strength. In the case of a vertical magnetic field, a larger strength of 0.4 T was required for highly aligned lamellar walls and larger channel widths. Compression strength tests indicated that the application of magnetic fields led to more homogeneously aligned channels, which resulted in increased compression strength in the longitudinal (parallel to the ice growth) direction. Applying a vertical magnetic field of 0.4 T with a cooling rate of 2 °C/min during the freezing step of the magnetic field-assisted freeze-casting method was found to result in the best conditions for producing highly anisotropic structures with large channel widths and fewer mineral bridges, which led to an increase in the mechanical strength.

1. Introduction

Boron carbide (B_4C) is one of the most attractive ceramic materials for a wide range of applications, from scaffolds to shielding structures, due to very promising physical and mechanical properties such as high hardness, good elastic modulus, high melting point, light weight, and good chemical stability [1,2]. Porous B_4C structures and their metal/B_4C composite counterparts can be used to create ultra-lightweight materials with excellent mechanical properties [3,4]. It has been shown that highly aligned porous preforms, especially in parallel to the channel direction, can significantly enhance the mechanical properties of resulting composites [3–5]. Although many different methods have been used to design porous ceramic structures, one of the most interesting methods that allows more precise control of the porosity and composition is the freeze-casting method [6–9]. Recently, we have shown that the freeze-casting method can be better controlled by applying a magnetic field to create more highly-aligned porous structures [10,11]. To make the magnetic field effective, the initial ceramic slurry was modified by mixing in small amounts of magnetic powders, for example Fe_3O_4, which facilitated the material alignment under applied magnetic field [10,12]. This resulted in a ceramic with a high degree of porosity, larger pore sizes, and an open cell structure that was promising for the fabrication of high fracture toughness metal matrix composites (MMCs) via full metal infiltration of the molten metal [3,13–15]. The resulting MMCs demonstrated great potential for being used in many industrial applications that require light weight, high strength, and high hardness [3,4].

To date, only a few studies have focused on the fabrication of B_4C structures using the freeze-casting method [16,17]. Wang et al. [17] used the freeze-casting method to fabricate aligned lamellar porous B_4C ceramics, with Al_2O_3–Y_2O_3 as the sintering additive. They found that the wavelength, lamellar thickness, and pore size decreased as the

* Corresponding author.
** Corresponding author.
E-mail addresses: SaidBakkar@my.unt.edu (S. Bakkar), marcus.young@unt.edu (M.L. Young).
[1] Present Address: Physics Department, University of Dallas, Irving, TX, USA.

https://doi.org/10.1016/j.ceramint.2021.11.226
Received 11 September 2021; Received in revised form 8 November 2021; Accepted 23 November 2021
Available online 25 November 2021

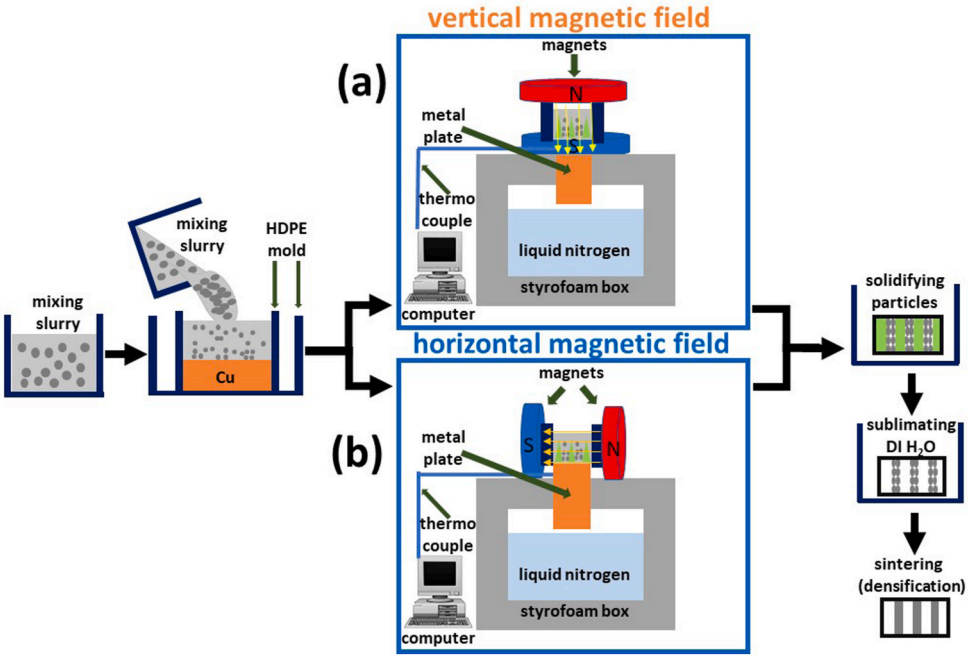

Fig. 1. Schematic diagram illustrating the magnetic freeze-casting method in cooling rate mode under two different magnetic field orientations: (a) Vertical magnetic field and (b) Horizontal magnetic field.

Al_2O_3–Y_2O_3 content increased. While pressureless sintering of B_4C with particle sizes <3 μm was typically being performed at temperatures between 2250 and 2350 °C [18–20], the use of different additives with B_4C, including TiC, SiC, C, and Y_2O_3/Al_2O_3, improved the sintering of the green bulk structures and reduced the sintering temperature [21–23]. Wang et al. [17] worked to improve the sintering of porous B_4C structures using freeze-casting, and found that adding varying amounts of 4–12 wt% of Al_2O_3–Y_2O_3 ceramic powder as sintering additives lowered the sintering temperature to 1900 °C, while aiding in the densification of the B_4C scaffold. In addition, they found that the compressive strength of the scaffolds was higher parallel to the ice growth direction when compared to perpendicular the ice growth direction. The use of magnetic powders, such as Fe_3O_4, for modifying the freeze-casting method [11], has also been previously reported to strengthen ceramics such as TiO_2 [10].

In this study, we created, for the first time, anisotropic porous B_4C structures with unidirectionally-elongated channels and large pore sizes using the magnetic field-assisted freeze-casting method. The B_4C was modified by adding of Fe_3O_4 to help in three distinct ways: 1) increasing the effectiveness of the magnetic field, 2) improving the sintering process by lower the sintering temperature and increasing the wetting between particles, and 3) acting as a strengthening component for the pure B_4C phase. This study was, therefore, focused on investigating the effects of the cooling rate, freezing time, magnetic field strength, and direction on the morphology (pore size, distribution, and alignment) and mechanical properties of the designed porous B_4C structures.

2. Experimental details

2.1. Materials

B_4C powder of 99.9% purity with a particle size of 1–3 μm (US Research Nanomaterials, Inc. Houston, TX, USA) was used as the dominant ceramic material in the slurry. Deionized water (DI H_2O) was used as the solvent. Polyvinyl alcohol (PVA, ≥ 99.0% purity, Sigma-Aldrich Co., St. Louis, MO, USA) at 3 wt% was premixed with the DI H_2O at 80 °C in B_4C to improve the ceramic powder bonding during freeze casting. Fe_3O_4 nanoparticles of 99.5% purity with a particle size of 15–20 nm (US Research Nanomaterials, Inc. Houston, TX, USA) were mixed with the slurry at 6 wt% of the total ceramics powder amount (including B_4C and the other additives) to investigate the effect of the magnetic field on the resulting porous structure.

2.2. Magnetic field-assisted freeze-casting

10 vol% B_4C solids loading, 90 vol% DI H_2O (with 3 wt % PVA as a binder), and 6 wt% of Fe_3O_4 of the ceramic powder amount as a magnetic material additive were mixed together to create highly-aligned porous B_4C scaffolds. The slurry was mixed using a laboratory Cole-Parmer ultra-compact digital mechanical mixer at a low speed of 120 rpm for 1 h to reduce formation of bubbles. The freeze casting process was initiated after mixing the slurry and pouring it at 3 °C into a 25.4 mm diameter cylindrical high-density polyethylene (HDPE) polymer mold attached to the bottom of a cold Cu plate in cooling rate mode [9]. Neodymium permanent disk magnets, each with a diameter of 32 mm and a thickness of 3.175 mm and a remanence of 1.44 T, were positioned two different ways: (1) vertically to form a uniform vertical magnetic field (parallel to the ice growth direction; Fig. 1 (a)) and (2) horizontally to form uniform a horizontal magnetic field (perpendicular to the ice growth direction; Fig. 1 (b)). The magnetic field was applied after pouring the slurry into the mold until complete freezing. The magnetic field strength, B, at the center of the gap between magnets for different numbers of magnet pairs (1, 2, and 3 magnet pairs) was calculated using the manufacturer's software (K & J Magnetic, Inc. software) [11]. By changing the distance between the magnets and the number of magnet pairs (1, 2, or 3), the magnetic field strength at the center of the samples was varied between 0.1 and 0.4 T. To avoid any particle migration or agglomeration near the permanent magnets, 3 mm thick layers near the surface of the samples were removed after sintering using the procedure described in the following references [11,15]. It is important to note that based on the results in Bakkar et al. [15], Fe_3O_4 particles were well dispersed throughout the samples.

2.3. Sublimating and sintering

After freezing the slurry, the frozen solvent was sublimated using a

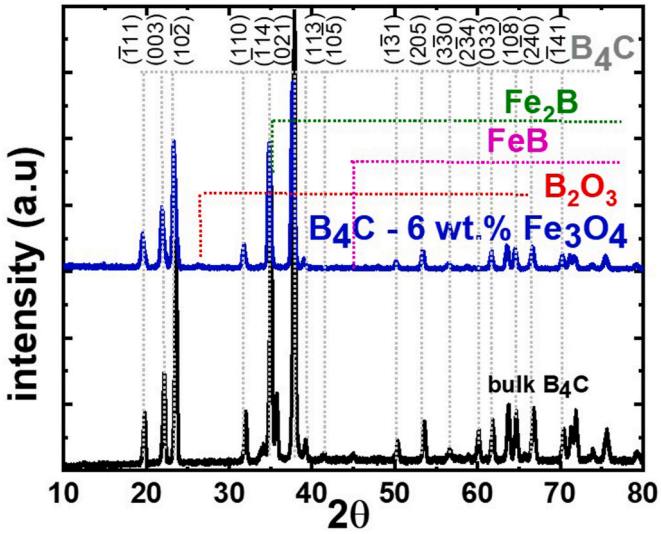

Fig. 2. XRD patterns of bulk B_4C and porous B_4C with 6 wt% Fe_3O_4 produced with magnetic field-assisted freeze-casting and sintered at 2000 °C for 2 h.

freeze dryer (LABCONCO Corporation, FreeZone 4.5 plus, Kansas City, MO, USA) in vacuum (pressure of 0.05 mbar) at −86 °C for 24 h. The sublimated sample was then sintered using a graphite hot zone furnace (1000-2560-FP20, Thermal Technology Inc.) in an ultra-high purity argon environment after vacuuming it to 10^{-5} torr. Sintering was conducted in a graphite furnace under an Ar environment, using the following steps: (1) burn off the PVA at 600 °C for 1 h, (2) sinter the ceramic powders (2000 °C with a hold for 2 h), and (3) furnace cool at a rate of 5 °C/min down to room temperature. The resulting average sample dimensions were 25.4 mm diameter and ~10 mm thickness.

2.4. Characterization

Surface morphology of the freeze-cast samples was characterized using the Hitachi Tabletop ESEM TM3030Plus (table-top SEM equipped with EDS). The average channel widths and porosities of the scaffolds were measured from the SEM images of the freeze-cast samples using ImageJ software. The crystallography X-ray diffraction (XRD) measurements were collected using a Rigaku Ultima III diffractometer with a Cu Kα radiation source at a scanning rate of 3°/min. The X-ray microscopy (XRM) micrographs of the sample were performed by using a Zeiss Xradia Versa 520 microscope to collect 3D images of the samples and examine the homogeneity of the channel alignment. For this, samples with a volume of $3 \times 3 \times 3$ mm^3 were scanned. The compression tests of the sintered samples were performed using a Shimadzu AGS-X loading frame equipped with a 10 kN load cell at a stroke rate of 2% of sample thickness mm/min. Three tests were conducted per sample for a total of two samples per processing condition.

3. Results and discussion

The XRD patterns of bulk B_4C and porous B_4C with 6 wt% Fe_3O_4 produced via magnetic field-assisted freeze-casting and sintered at 2000 °C for 2 h are shown in Fig. 2. The XRD spectra indicated that B_4C was the primary phase in the samples. The B_4C-6 wt.% Fe_3O_4 samples revealed two additonal phases, FeB and Fe_2B, which were expected, given the composition and thermal history of the sample [24]. These two intermetallic phases (FeB, Fe_2B) indicated that the oxygen in Fe_3O_4 was reduced, allowing for Fe to react with the B_4C. The presence of an Fe-rich Fe_2B phase indicated that diffusion was limited due to the sintering time and temperature, as the equilibrium FeB phase was also present [25,26].

3.1. Influence of the direction and strength of the magnetic field

Fig. 3 shows the top view of SEM micrographs for B_4C samples in the green state produced with a vertically-applied magnetic field strength of (a) 0, (b) 0.3, and (c) 0.4 T, respectively, via the magnetic field-assisted freeze-casting method using a slurry consisting of 10 vol% B_4C, 3 wt% PVA, and 6 wt% Fe_3O_4, and a cooling rate of 0.7 °C/min. Fig. 3 (d) summarizes the channel width distributions and mean values for the resulting porous B_4C structures, as calculated from the SEM images using ImageJ software. Samples produced without a magnetic field showed randomly oriented porous channels with a porosity of 55% and a channel width of 38 ± 10 μm. Samples produced with a 0.3 T vertical magnetic field demonstrated partially-aligned channel walls with a slightly larger porosity (59%) and a channel width of 44 ± 12 μm. Samples produced with a vertically-applied magnetic field of 0.4 T indicated complete alignment of the channel walls, an increased channel width of 46 ± 16 μm, and a higher porosity of 70%. This result was in agreement with previous results for the Al_2O_3 system [11]. To evaluate the alignment of the channel walls, channel angles were measured using ImageJ software for the samples produced using a vertical magnetic field of 0, 0.3, and 0.4 T. A minimum of 60 measurements were collected for each sample. The average measured angles for the samples produced under 0, 0.3, and 0.4 T were found to be 39.6° ± 27°, 21.4° ± 23°, and 4.5° ± 2°, respectively. Hence, near-perfect alignment, i.e. (~0° off of perfect alignment with the direction of the magnetic field) was achieved for samples produced using a vertically-applied magnetic field of 0.4 T.

Fig. 4 shows SEM micrographs from the top view of B_4C samples in the green state with a horizontally-applied magnetic field strength of (a) 0.1, (b) 0.2, and (c) 0.3 T, respectively. These samples were produced via magnetic field-assisted freeze-casting using the same slurry content and cooling rate (0.7 °C/min). Fig. 4 (d) summarizes the channel width distributions and mean values for the resulting porous B_4C structures, as calculated from the SEM images using ImageJ software. The SEM images in Fig. 4 (a-c) suggest that the porous channels became more aligned with an increase in horizontal magnetic field strength. In addition, the magnetic field enhanced alignment of minor bridges between lamellar walls, which was in agreement with the results reported in previous studies on hydroxyapatite, ZrO_2, Al_2O_3, TiO_2, and mixtures thereof [10,27,28]. The porosity and channel widths decreased with increasing horizontally-applied magnetic field strength, from 62% to 38 ± 11 μm to 56% and 33 ± 8 μm, and to 46% and 15 ± 5 μm for 0.1, 0.2, and 0.3 T, respectively. Since the channel width was significantly decreased, we decided not to examine 0.4 T. It is clear though that the alignment is improving with increasing magnetic field. In addition, the homogeneity of the samples increased with increasing horizontally-applied magnetic field strength, as shown in the distribution graphs (Fig. 4 (d)). The results shown in Figs. 3 and 4 indicate that a weak horizontal magnetic field is sufficient to align the minor bridges, and thus, the porous channels, while a stronger vertical magnetic field of 0.4 T is required to align the lamellar walls and channels. Interestingly, the porosity increased with an increase in vertically-applied magnetic field strength, but decreased with an increase in horizontally-applied magnetic field strength. These results indicated that the best conditions to produce B_4C with highly-aligned porous channels and large channel widths can be achieved using a vertically-applied magnetic field strength of 0.4 T. It should be noted that we only show representative samples here (Figs. 3 and 4), but many more samples were produced in each condition to verify the alignment and confirm the effect of the magnetic field during freeze-casting.

Compression tests were conducted on samples produced under various vertically- or horizontally-applied magnetic field strengths after sublimation and sintering at 2000 °C for 2 h. Fig. 5 shows the representative compression stress-strain curves of the sintered samples in the longitudinal direction (parallel to the ice growth direction). Compression test results for samples prepared using vertical magnetic fields of 0, 0.3, and 0.4 T (Fig. 5 (a)), and horizontal magnetic fields of 0, 0.2, and

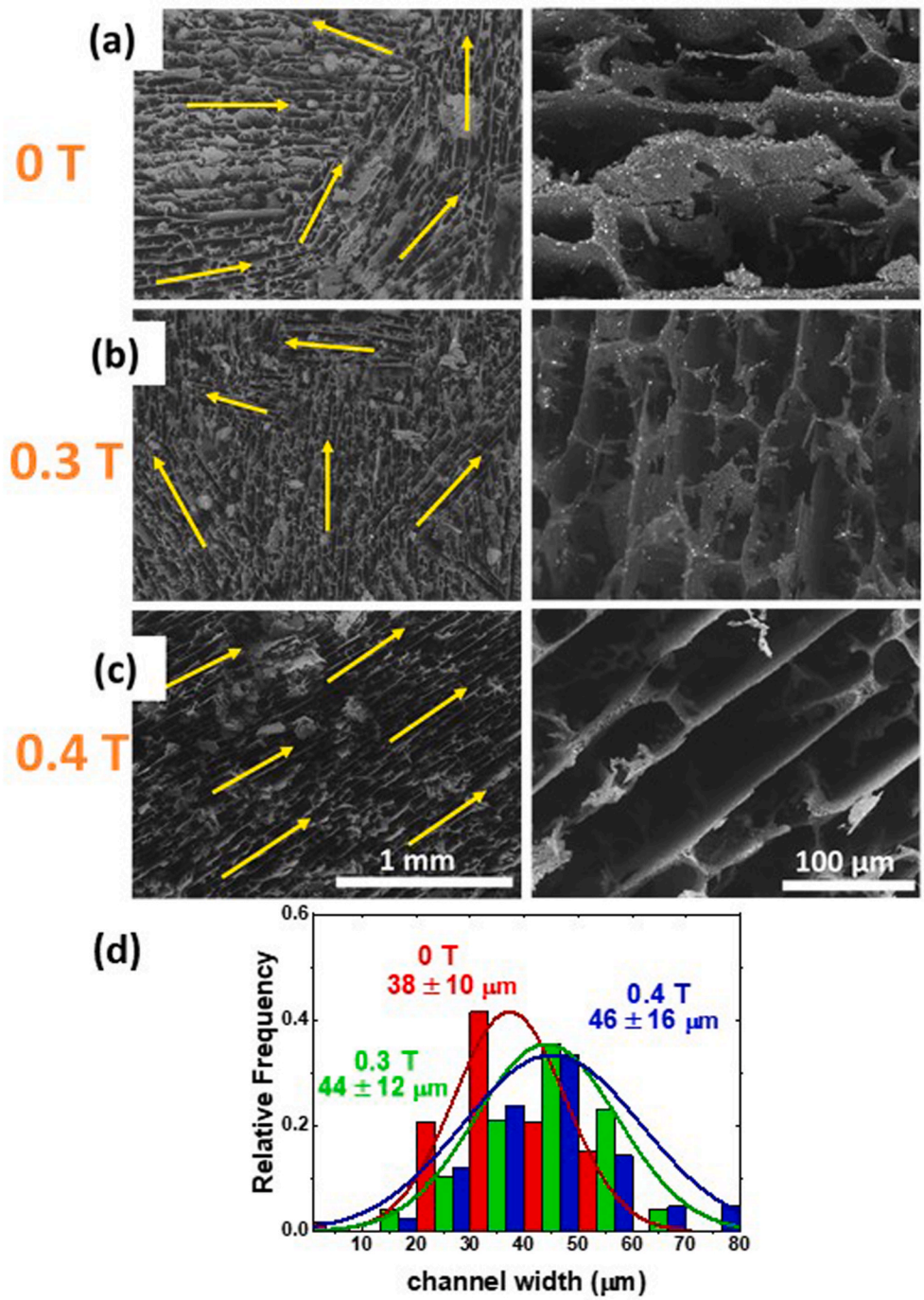

Fig. 3. SEM micrographs of the top view of porous B_4C samples in the green state produced via freeze-casting method under applied vertical magnetic field strengths of (a) 0, (b) 0.3, and (c) 0.4 T, respectively (the yellow arrows show the direction of aligned channel walls). (d) Graph of channel width distributions and their mean values for the porous B_4C samples under vertically-applied magnetic fields of 0, 0.3, and 0.4 T (measured from the middle regions), respectively, as calculated from the SEM images using ImageJ software. (For interpretation of the references to colour in this figure legend, the reader is referred to the Web version of this article.)

0.3 T (Fig. 5 (b)). Fig. 5 (a and b) showed that the compression strengths of samples produced under magnetic fields were higher than for those produced under no magnetic field. The general trend was that higher magnetic field strength (regardless of whether it was vertically- or horizontally-applied) led to higher compression strength in the longitudinal direction (parallel to the ice growth), which was likely due to better and more homogeneous alignment of the ceramic columns. The compression strength test was selected in the longitudinal direction because it is in the direction that provides a larger strength as per the various results reported in the literature (the highest compression strength was in the direction of ice growth) [10,12,17]. One exception was for the samples produced under vertical magnetic fields of 0.3 and 0.4 T, respectively, where the compression strength was higher under 0.3 T as compared to 0.4 T. This was likely due to the lower porosity (59%) and smaller average channel size (39 ± 11 μm) for the 0.3 T sample as compared to the 70% porosity and 46 ± 11 μm average channel size for the 0.4 T sample. Fig. 5 (c) illustrates the influence of porosity and channel size on the ultimate compression strength in the longitudinal direction (parallel to the ice growth direction). As expected, higher porosity and larger channel size resulted in lower compression strength, which was in a good agreement with other studies on porous B_4C produced by the freeze-casting method [16,17,29]. Furthermore, the ultimate compression strengths of samples produced using a horizontally-applied magnetic fields were higher than those produced using a vertically-applied magnetic field. This result likely occurs for two reasons. First, the horizontal magnetic field works to align the

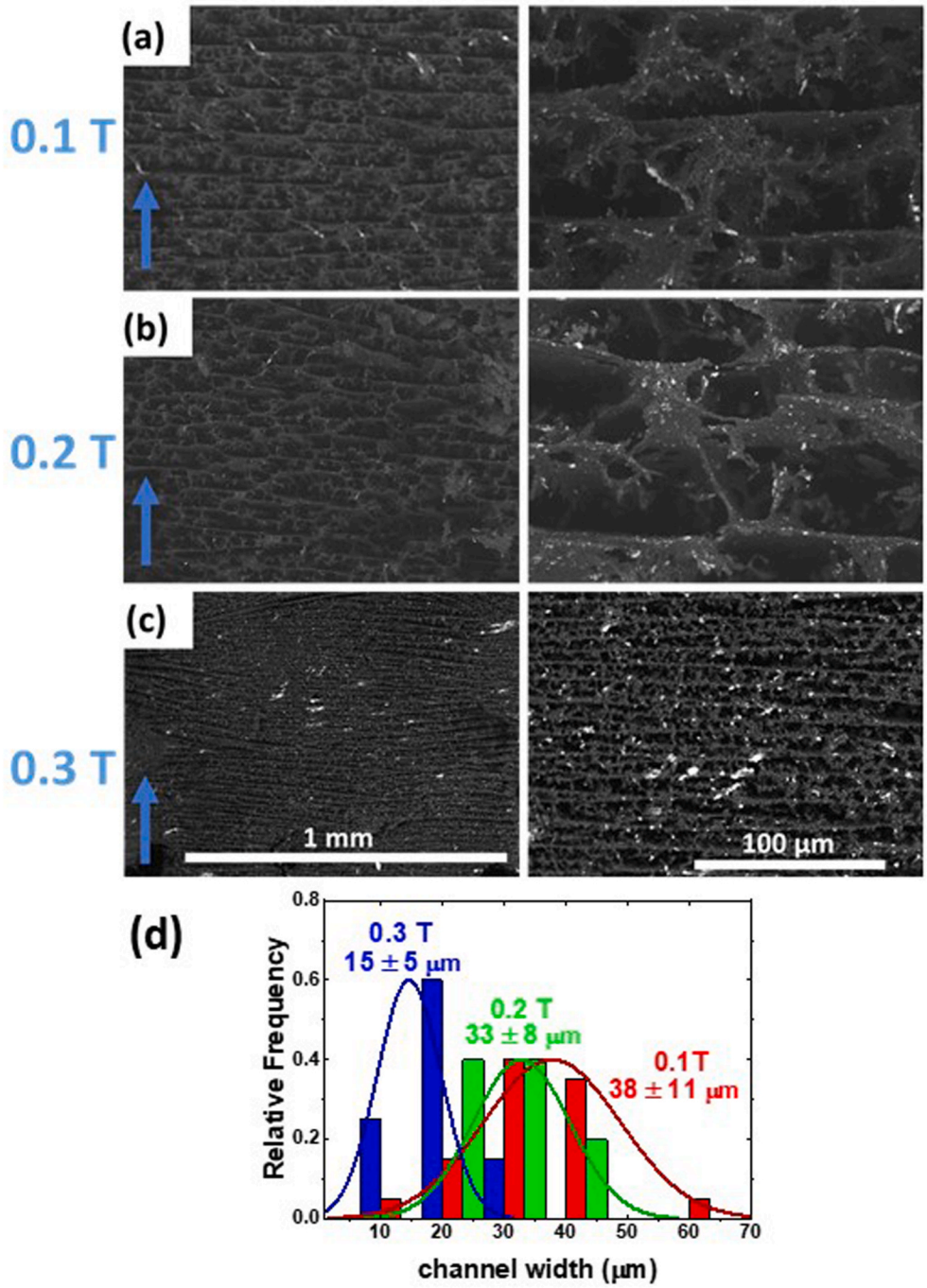

Fig. 4. SEM micrographs of the top view of the porous B_4C samples in the green state produced via freeze-casting method under applied horizontal magnetic field strengths of (a) 0.1, (b) 0.2, and (c) 0.3 T, respectively. (d) Graph of channel width distributions and their mean values for the porous B_4C samples under horizontally-applied magnetic fields of 0.1, 0.2, and 0.3 T (measured for the middle regions), respectively, as calcualted from the SEM images using ImageJ software. (For interpretation of the references to colour in this figure legend, the reader is referred to the Web version of this article.)

mineral bridges, and helps to build more minor bridges between the lamellar walls, which results in enhanced compression strength and mechanical properties [27,28,30,31]. Second, the porosities of samples produced using a horizontally-applied magnetic field was lower than those produced using a vertically-applied magnetic field, which led to a higher density of B_4C and an increase in compressive strength (Fig. 5 (c)) [17,27,28,30,31].

In general, the strength of a porous ceramic is affected by many factors, including density, porosity, specimen size, and the presence of micro-defects [32]. While not performed here, a Weibull distribution function would also be recommended for a more comprehensive understanding of compression strength in ceramics, whereby compression data is collected from a group of specimens with the same material, size, fabrication conditions, and loading conditions [32].

3.2. *Influence of cooling rate and freezing time*

To investigate the effects of cooling rate and freezing time on porous B_4C structures, three different samples were prepared under identical conditions using magnetic field-assisted freeze-casting, in particular, at vertical magnetic field of 0.4 T, while only changing the cooling rate used during the freezing step. Fig. 6 (a) shows a plot of temperature as a function of time at three different cooling rates (0.8, 2, and 4 °C/min) for porous B_4C samples, which were produced using the magnetic field-assisted freeze-casting method under a vertically-applied magnetic field strength of 0.4 T. Fig. 6 (b) shows SEM micrographs from the top view for these three samples. The results indicated that the samples produced using the lowest cooling rate (0.8 °C/min) had a high density of mineral bridges. A similar result was observed in the samples

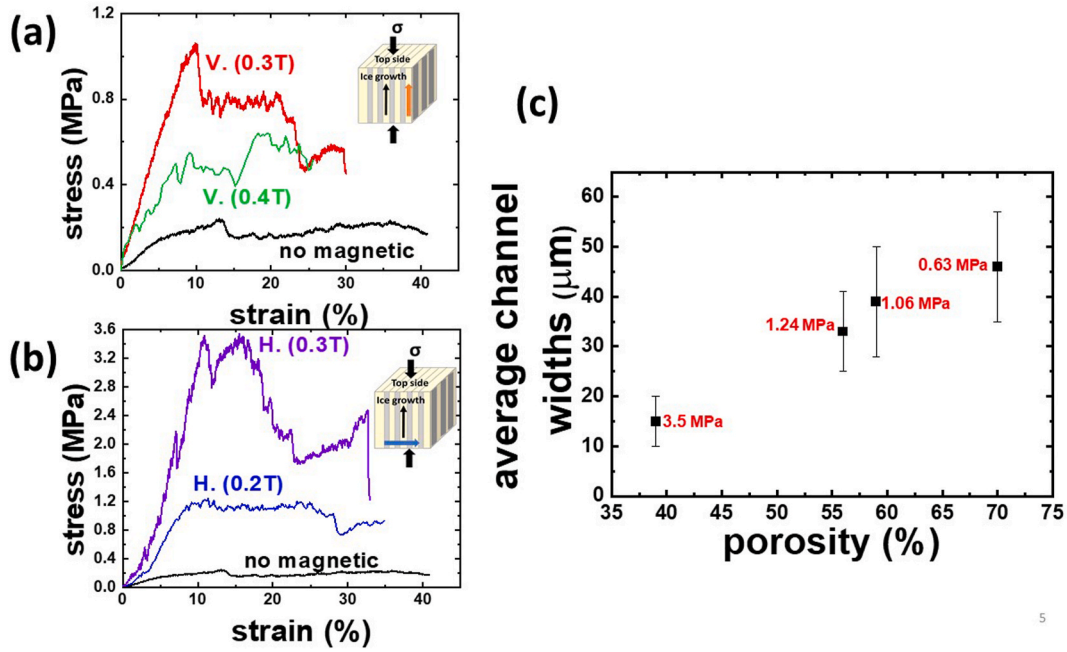

Fig. 5. Representative compression stress-strain curves of sintered porous B_4C ceramic structures in the longitudinal direction, i.e. solidification direction (parallel to the ice growth direction) prepared by (a) Vertically-aligned magnetic field-assisted freeze-casting (orange arrow) and (b) Horizontally-aligned magnetic field-assisted freeze-casting (blue arrow). The inset figures show the compression test and magnetic field directions (orange and blue arrows). (c) Effect of porosity and the average channel widths on ultimate compression strength (values in red). (For interpretation of the references to colour in this figure legend, the reader is referred to the Web version of this article.)

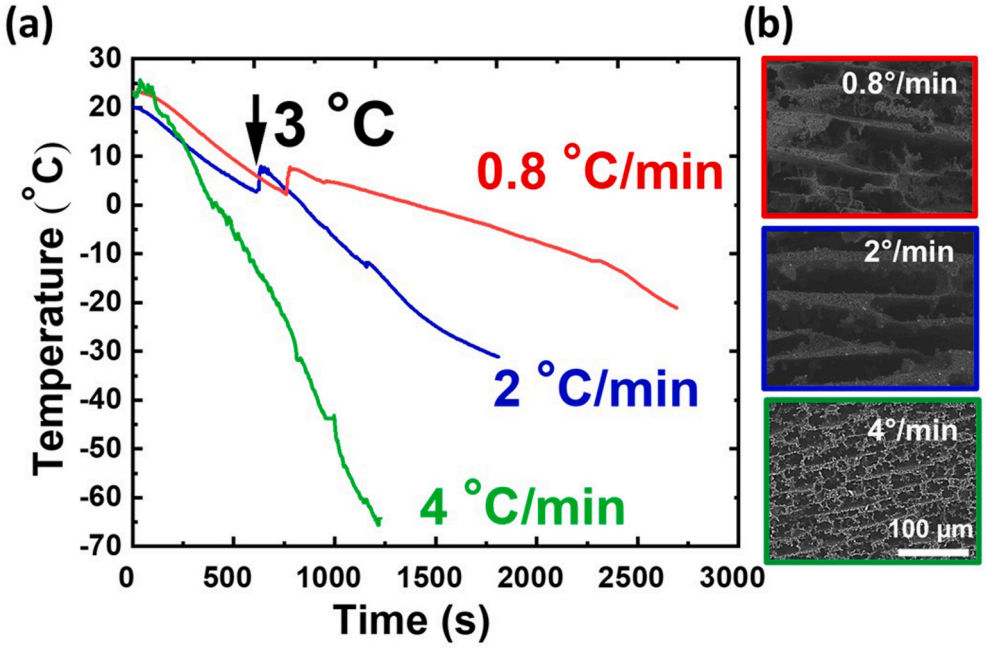

Fig. 6. Influence of different cooling rates and corresponding freezing time on the structures of sintered B_4C samples produced under a vertically-aligned magnetic field of 0.4 T. (a) Graphs of temperature as a function of time for three different cooling rates (0.8, 2, and 4 °C/min) (b) Corresponding SEM micrographs of samples from the top view. The temperature 3 °C is noted as this is temperature at which the slurry is added at the start of freezing.

produced under a cooling rate of 0.7 °C/min, as shown in Fig. 3 (c). Samples produced under high cooling rates (4 °C/min) demonstrated a high density of dendrites between the lamellar walls, while samples produced under cooling rates of 2 °C/min had smooth lamellar walls and clear open channels. The temperature versus time graphs indicated that it took approximately 1250, 1800, and 2750 s to completely freeze samples with a thickness of ~10 mm using 4, 2, and 0.8 °C/min cooling rates, respectively. The resulting ice front velocity (ν) values of 8.0, 5.6, and 3.6 μm/s, respectively, were calculated by dividing the thicknesses of the samples by the freezing times. The average wavelengths (channel widths and adjacent wall thicknesses) estimated by analyzing the SEM images via ImageJ were 19 ± 4 μm, 44 ± 9 μm, 48 ± 8 μm, under cooling rates of 4, 2, and 0.8 °C/min, respectively. It was observed that as the ice front velocity increased, the widths of the channels, the structures of the

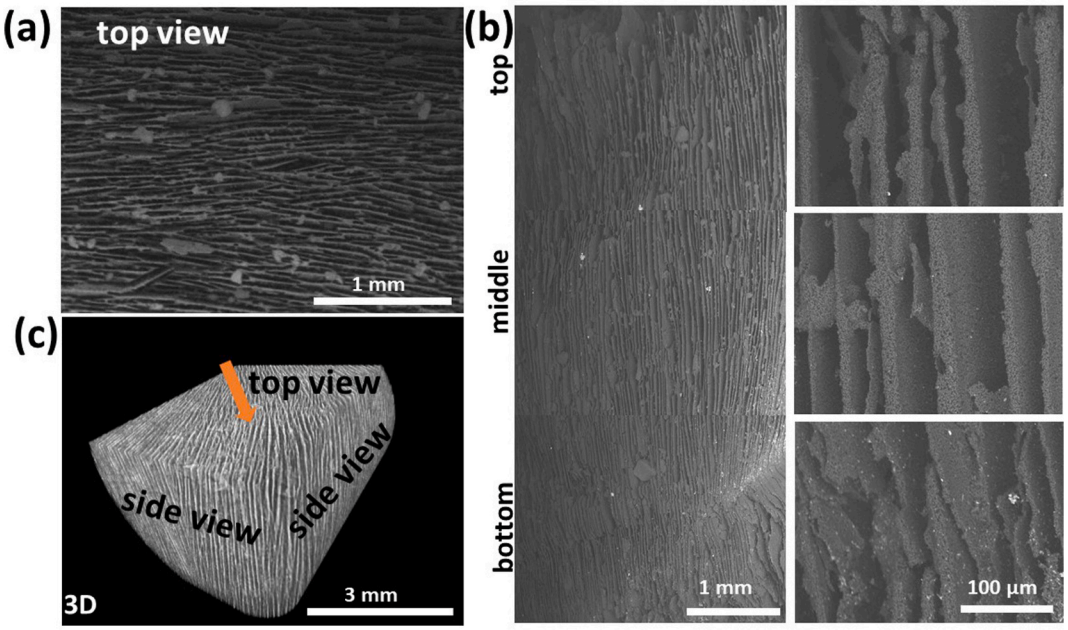

Fig. 7. SEM micrographs and XRM scan images of the sintered B_4C sample produced by magnetic field-assisted freeze-casting under a vertically-applied magnetic field of 0.4 T and a cooling rate of 2 °C/min. (a) Top view (perpendicular to the ice growth) (b) Cross-sectional view (parallel to the ice growth direction) of top, middle, and bottom regions of the sample (c) 3D XRM scan image (orange arrow represents the magnetic field direction). (For interpretation of the references to colour in this figure legend, the reader is referred to the Web version of this article.)

wavelengths, and the wall thicknesses decreased, which suggested that the faster freezing rate led to the finer overall microstructures [33,34].

Fig. 7 shows SEM micrographs of the top and side views of the sample (top, middle, and bottom regions), as well as the XRM scan of the sintered porous B_4C structure. As illustrated in Fig. 7 (a-b), the top and side view SEM images show that the porous B_4C structure exhibits excellent alignment of the channels and large channel widths. Fig. 7 (c) shows a 3D image of the sample measured by the XRM scan. It further confirms the homogeneity and strong alignment of channels throughout the thickness of the sample in all directions, as demonstrated by the top view (perpendicular to the ice growth direction) and the side view (parallel to the ice growth direction) images. Thus, the application of a 0.4 T magnetic field with a cooling rate of 2 °C/min resulted in a ~10 mm thick uniform sample with well-aligned porous channels throughout the sample.

Based on the aforementioned observations, the homogeneity of the most promising structure, containing large, clear open channels and smooth lamellar walls, was further evaluated. This sintered porous B_4C specimen was produced under the following conditions:

1 Mixing a slurry consisting of 10 vol% B_4C, 90 vol% DI H_2O, 3 wt% PVA, and 6 wt% Fe_3O_4.
2 Applying a vertical magnetic field strength of 0.4 T at the freezing temperature.
3 Using a cooling rate of 2 °C/min.

4. Conclusions

For the first time, porous B_4C structures were successfully produced using the magnetic field-assisted freeze casting method. Samples under applied magnetic field showed stronger anisotropy in the channel directions and resulted in larger channel sizes. The effect of magnetic field direction and strength was also explored as a means to control the resulting porous ceramic structures. The following results were found:

1 A vertically-applied magnetic field of 0.4 T (compared to 0 and 0.3 T fields) generated a uniform uniaxial alignment of channels throughout the samples, with large average channel sizes.
2 Weak horizontal magnetic fields of 0.1, 0.2, and 0.3 T were sufficient to align channels and mineral bridges between the lamellar walls. Additionally, channel widths decreased as magnetic field strength was increased. In contrast, the application of a stronger vertically-applied magnetic field resulted in the development of larger, well-aligned channels.
3 Compressive strength tests in the longitudinal direction (parallel to the ice growth) demonstrated that the structures of samples produced under magnetic fields was stronger than those produced under no magnetic fields, due to more homogeneously aligned channels and minor bridges between the walls. Also, structures with higher porosities and larger channel sizes resulted in a lower compression strength.
4 A cooling rate of 2 °C/min (compared to 0.8 and 4 °C/min) was able to reduce the densities of dendrites and minor bridges between the lamellar walls. XRM scan results confirmed that application of a 0.4 T magnetic field with a cooling rate of 2 °C/min resulted in a uniform structure with well-aligned porous channels throughout the sample.

This work has demonstrated a promising method for using vertical magnetic field-assisted freeze-casting to produce porous B_4C structures with large, highly aligned channels. These preforms can be infiltrated with molten metals to produce unique MMCs.

Declaration of competing interest

The authors declare that they have no known competing financial interests or personal relationships that could have appeared to influence the work reported in this paper.

Acknowledgments

The authors thank Dr. Sheldon Shi and Mr. Lee Smith for assistance with mechanical (compression) testing. This work was performed in part

at the University of North Texas's (UNT) Materials Research Facility (MRF) and at UNT's Advanced Materials and Manufacturing Processes Institute (AMMPI). This research was supported by DEVCOM-Army Research Laboratory (Award No. W911NF-19-2-0011).

References

[1] F. Thévenot, Boron carbide-A comprehensive review, J. Eur. Ceram. Soc. 6 (1990) 205–225, https://doi.org/10.1016/0955-2219(90)90048-K.
[2] S. Yamada, K. Hirao, Y. Yamauchi, S. Kanzaki, B 4 C À CrB 2 Composites with Improved Mechanical Properties, vol. 23, 2003, pp. 561–565.
[3] X.F. Tan, F.H. Zeng, S.Q. Wang, F. Zhou, X. Xiong, Effects of heat treatment on phase contents and mechanical properties of infiltrated B4C/2024Al composites, Trans. Nonferrous Met. Soc. China (English Ed. 24 (2014) 2359–2365, https://doi.org/10.1016/S1003-6326(14)63357-4.
[4] Z.L. Chao, L.T. Jiang, G.Q. Chen, J. Qiao, Q. Z, Z.H. Yu, Y.F. Cao, G.H. Wu, The microstructure and ballistic performance of B 4 C/AA2024 functionally graded composites with wide range B 4 C volume fraction, Compos. B Eng. 161 (2019) 627–638, https://doi.org/10.1016/j.compositesb.2018.12.147.
[5] Ş. Karabulut, H. Karakoç, R. Çıtak, Influence of B4C particle reinforcement on mechanical and machining properties of Al6061/B4C composites, Compos. B Eng. 101 (2016) 87–98, https://doi.org/10.1016/j.compositesb.2016.07.006.
[6] S. Deville, Freeze-casting of porous biomaterials: structure, properties and opportunities, Materials (Basel) 3 (2010) 1913–1927, https://doi.org/10.3390/ma3031913.
[7] K.L. Scotti, D.C. Dunand, Freeze casting – a review of processing, microstructure and properties via the open data repository, FreezeCasting.net, Prog. Mater. Sci. 94 (2018) 243–305, https://doi.org/10.1016/j.pmatsci.2018.01.001.
[8] T. Moritz, H.J. Richter, Ceramic bodies with complex geometries and ceramic shells by freeze casting using Ice as mold material, J. Am. Ceram. Soc. 89 (2006) 2394–2398, https://doi.org/10.1111/j.1551-2916.2006.01081.x.
[9] S. Bakkar, M.V. Pantawane, J.J. Gu, A. Ghoshal, M. Walock, M. Murugan, M. L. Young, N. Dahotre, D. Berman, S.M. Aouadi, Laser surface modification of porous yttria stabilized zirconia against CMAS degradation, Ceram. Int. 46 (2020), https://doi.org/10.1016/j.ceramint.2019.11.061.
[10] M.M. Porter, M. Yeh, J. Strawson, T. Goehring, S. Lujan, P. Siripasopsotorn, M. A. Meyers, J. McKittrick, Magnetic freeze casting inspired by nature, Mater. Sci. Eng. 556 (2012) 741–750, https://doi.org/10.1016/j.msea.2012.07.058.
[11] S. Bakkar, J. Lee, N. Ku, D. Berman, S.M. Aouadi, R.E. Brennan, M.L. Young, Design of porous aluminum oxide ceramics using magnetic field-assisted freeze-casting, J. Mater. Res. 35 (2020) 1–11, https://doi.org/10.1557/jmr.2020.197.
[12] P. Niksiar, F. Su, M. Frank, T. Ogden, S. Naleway, M. Meyers, J. McKittrick, M. Porter, External field assisted freeze casting, Ceramics 2 (2019) 208–234, https://doi.org/10.3390/ceramics2010018.
[13] Q. Liu, F. Ye, Y. Gao, S. Liu, H. Yang, Z. Zhou, Fabrication of a new SiC/2024Al co-continuous composite with lamellar microstructure and high mechanical properties, J. Alloys Compd. 585 (2014) 146–153, https://doi.org/10.1016/j.jallcom.2013.09.140.
[14] A. Shaga, P. Shen, R.F. Guo, Q.C. Jiang, Effects of oxide addition on the microstructure and mechanical properties of lamellar SiC scaffolds and Al-Si-Mg/SiC composites prepared by freeze casting and pressureless infiltration, Ceram. Int. 42 (2016) 9653–9659, https://doi.org/10.1016/j.ceramint.2016.03.052.
[15] S. Bakkar, M. Wall, N. Ku, D. Berman, S.M. Aouadi, R.E. Brennan, M.L. Young, Al/Al2O3 metal matrix composites produced using magnetic field-assisted freeze-casting of porous ceramic structures, J. Mater. Res. (2021), https://doi.org/10.1557/s43578-021-00159-9.
[16] Y. Wang, Q. Liu, B. Zhang, H. Zhang, Y. Jin, Z. Zhong, F. Ye, W. Wang, Structure/processing relationships and mechanical properties of freeze-cast B4C scaffolds with unidirectional channels, J. Mater. Sci. 56 (2021) 13989–14000, https://doi.org/10.1007/s10853-021-06236-y.
[17] Y. Wang, Q. Liu, B. Zhang, J. Ding, H. Zhang, Y. Jin, Z. Zhong, W. Wang, F. Ye, Controlling the structure and mechanical properties of porous B4C ceramics with unidirectionally aligned channels using sintering additives, Ceram. Int. 46 (2020) 17117–17121, https://doi.org/10.1016/j.ceramint.2020.03.218.
[18] R.M. Da Rocha, F.C.L. De Melo, Sintering of B4C by pressureless liquid phase sintering, Mater. Sci. Forum 660–661 (2010) 170–175. https://doi.org/10.4028/www.scientific.net/MSF.660-661.170.
[19] H. Lee, R.F. Speyer, W.S. Hackenberger, Sintering of boron carbide heat-treated with hydrogen, J. Am. Ceram. Soc. 85 (2002) 2131–2133, https://doi.org/10.1111/j.1151-2916.2002.tb00420.x.
[20] M. Mashhadi, E. Taheri-Nassaj, V.M. Sglavo, Pressureless sintering of boron carbide, Ceram. Int. 36 (2010) 151–159, https://doi.org/10.1016/j.ceramint.2009.07.034.
[21] R. Wei, Y. Zhang, H. Gong, Y. Jiang, Y. Zhang, The effects of rare-earth oxide additives on the densification of pressureless sintering B4C ceramics, Ceram. Int. 39 (2013) 6449–6452, https://doi.org/10.1016/j.ceramint.2013.01.073.
[22] X. Du, Z. Zhang, W. Wang, H. Wang, Z. Fu, Microstructure and properties of B4C-SiC composites prepared by polycarbosilane-coating/B4C powder route, J. Eur. Ceram. Soc. 34 (2014) 1123–1129, https://doi.org/10.1016/j.jeurceramsoc.2013.10.039.
[23] X. Zhang, Z. Zhang, Y. Liu, A. Wang, S. Tian, W. Wang, J. Wang, High-performance B 4 C–TiB 2 –SiC composites with tuneable properties fabricated by reactive hot pressing, J. Eur. Ceram. Soc. 39 (2019) 2995–3002, https://doi.org/10.1016/j.jeurceramsoc.2019.04.001.
[24] Agency Japan Atomic Energy, 2020. https://thermodb.jaea.go.jp/data/en/pd/Fe-B4C.html.
[25] F. Nair, M. Hamamcı, Effect of in-situ synthesized boride phases on the impact behavior of iron-based composites reinforced by B4C particles, Metals (Basel) 10 (2020), https://doi.org/10.3390/met10050554.
[26] O. Ozdemir, M. Usta, C. Bindal, A.H. Ucisik, Hard iron boride (Fe2B) on 99.97 wt% pure iron, Vacuum 80 (2006) 1391–1395, https://doi.org/10.1016/j.vacuum.2006.01.022.
[27] M.M. Porter, P. Niksiar, J. McKittrick, Microstructural control of colloidal-based ceramics by directional solidification under weak magnetic fields, J. Am. Ceram. Soc. 99 (2016) 1917–1926, https://doi.org/10.1111/jace.14183.
[28] M.B. Frank, S.E. Naleway, T. Haroush, C.H. Liu, S.H. Siu, J. Ng, I. Torres, A. Ismail, K. Karandikar, M.M. Porter, O.A. Graeve, J. McKittrick, Stiff, porous scaffolds from magnetized alumina particles aligned by magnetic freeze casting, Mater. Sci. Eng. C 77 (2017) 484–492, https://doi.org/10.1016/j.msec.2017.03.246.
[29] Y. Wang, Q. Liu, B. Zhang, J. Ding, H. Zhang, Y. Jin, Z. Zhong, W. Wang, F. Ye, Effect of pretreatment process of B4C powder on the surface properties and freeze-cast porous ceramics, Mater. Chem. Phys. 251 (2020), 123209, https://doi.org/10.1016/j.matchemphys.2020.123209.
[30] M.B. Frank, S. Hei Siu, K. Karandikar, C.H. Liu, S.E. Naleway, M.M. Porter, O. A. Graeve, J. McKittrick, Synergistic structures from magnetic freeze casting with surface magnetized alumina particles and platelets, J. Mech. Behav. Biomed. Mater. 76 (2017) 153–163, https://doi.org/10.1016/j.jmbbm.2017.06.002.
[31] I. Nelson, T.A. Ogden, S. Al Khateeb, J. Graser, T.D. Sparks, J.J. Abbott, S. E. Naleway, Freeze-casting of surface-magnetized iron(II,III) oxide particles in a uniform static magnetic field generated by a helmholtz coil, Adv. Eng. Mater. 21 (2019) 1–11, https://doi.org/10.1002/adem.201801092.
[32] W.S. Lei, Z. Yu, P. Zhang, G. Qian, Standardized Weibull statistics of ceramic strength, Ceram. Int. (2020), https://doi.org/10.1016/j.ceramint.2020.10.073.
[33] S. Deville, E. Saiz, R.K. Nalla, A.P. Tomsia, Freezing as a path to build complex composites, Science 311 (80) (2006) 515–518, https://doi.org/10.1126/science.1120937.
[34] S. Deville, E. Saiz, A.P. Tomsia, Ice-templated porous alumina structures, Acta Mater. 55 (2007) 1965–1974, https://doi.org/10.1016/j.actamat.2006.11.003.